HAL
open science

Ring Shadowing Effects on Saturn's Ionosphere: Implications for Ring Opacity and Plasma Transport

Lina Hadid, M. W. Morooka, J.- E. Wahlund, L. Moore, T. E. Cravens, M. M. Hedman, N. J. T. Edberg, E. Vigren, J. H. Waite Jr., R. Perryman, et al.

To cite this version:

Lina Hadid, M. W. Morooka, J.- E. Wahlund, L. Moore, T. E. Cravens, et al.. Ring Shadowing Effects on Saturn's Ionosphere: Implications for Ring Opacity and Plasma Transport. Geophysical Research Letters, 2018, 45 (19), pp.10,084-10,092. 10.1029/2018GL079150 . hal-02640853

HAL Id: hal-02640853

https://hal.science/hal-02640853v1

Submitted on 16 Sep 2022

HAL is a multi-disciplinary open access archive for the deposit and dissemination of scientific research documents, whether they are published or not. The documents may come from teaching and research institutions in France or abroad, or from public or private research centers.

L'archive ouverte pluridisciplinaire **HAL**, est destinée au dépôt et à la diffusion de documents scientifiques de niveau recherche, publiés ou non, émanant des établissements d'enseignement et de recherche français ou étrangers, des laboratoires publics ou privés.

Geophysical Research Letters

RESEARCH LETTER
10.1029/2018GL079150

Special Section:
Cassini's Final Year: Science Highlights and Discoveries

Key Points:
- The D, C, and the Cassini Division are confirmed to be optically thin to extreme ultraviolet radiation, unlike the A and the B rings
- The total current collected by the Langmuir probe is lower at the inner part of the A ring compared to its outer part, consistent with the A ring normal optical depth properties
- The responses of the ionosphere to the B ring shadow is variable, implying different proton production rate and ionospheric plasma transport

Correspondence to:
L. Z. Hadid,
lina.hadid@irfu.se

Citation:
Hadid, L. Z., Morooka, M. W., Wahlund, J.-E., Moore, L., Cravens, T. E., Hedman, M. M., et al. (2018). Ring shadowing effects on Saturn's ionosphere: Implications for ring opacity and plasma transport. *Geophysical Research Letters*, *45*, 10,084–10,092. https://doi.org/10.1029/2018GL079150

Received 12 JUN 2018
Accepted 3 JUL 2018
Accepted article online 28 JUL 2018
Published online 4 OCT 2018

©2018. American Geophysical Union. All Rights Reserved.

Ring Shadowing Effects on Saturn's Ionosphere: Implications for Ring Opacity and Plasma Transport

L. Z. Hadid[1], M. W. Morooka[1], J.-E. Wahlund[1], L. Moore[2], T. E. Cravens[3], M. M. Hedman[4], N. J. T. Edberg[1], E. Vigren[1], J. H. Waite Jr.[5], R. Perryman[5], W. S. Kurth[6], W. M. Farrell[7], and A. I. Eriksson[1]

[1]Swedish Institute of Space Physics, Uppsala, Sweden, [2]Center for Space Physics, Boston University, Boston, MA, USA, [3]Department of Physics and Astronomy, University of Kansas, Lawrence, KS, USA, [4]Department of Physics, University of Idaho, Moscow, ID, USA, [5]Space Science and Engineering Division, Southwest Research Institute, San Antonio, TX, USA, [6]Department of Physics and Astronomy, University of Iowa, Iowa City, IA, USA, [7]NASA/Goddard Space Flight Center, Greenbelt, MD, USA

Abstract We present new results obtained by the Radio and Plasma Wave Science Langmuir probe on board Cassini during the Grand Finale. The total direct current sampled by the Langmuir probe at negative bias voltage is used to study the effect of the ring shadows on the structure of the Kronian topside ionosphere. The D and C rings and the Cassini Division are confirmed to be optically thin to extreme ultraviolet solar radiation. However, different responses from the opaque A and B rings are observed. The edges of the A ring shadow are shown to match the A ring boundaries, unlike the B ring, which indicates variable responses to the B ring shadow. We show that the variable responses are due to the ionospheric plasma, more precisely to the longer chemical lifetime of H^+ compared to H_2^+ and H_3^+, suggesting that the plasma is transported from the sunlit region to the shadowed one in the ionosphere.

Plain Language Summary As Saturn's northern hemisphere experienced summer during the Grand Finale, the planet's northern dayside hemisphere and its rings were fully illuminated by the Sun. However, the southern hemisphere was partly obscured because of the shadows cast by the A and B rings. Using the in situ measurements of the Langmuir probe part of the Radio and Plasma Wave Science investigation on board the Cassini spacecraft, we study for the first time the effect of the ring shadows on Saturn's ionosphere. From the ring shadows signatures on the total ion current collected by the Langmuir probe, we show that the A and B rings are optically thicker (to the solar extreme ultraviolet radiation) than the inner C and D rings and the Cassini Division to the solar extreme ultraviolet radiation. Moreover, we reproduce the boundaries of the A ring and the outer edge of the B ring. Furthermore, observed variations with respect to the inner edge of the B ring imply a delayed response of the ionospheric H^+ because of its long lifetime and suggest that the ionospheric plasma is transported from an unshadowed region to a shadowed one in the ionosphere.

1. Introduction

The classical ring system of Saturn, the A, B, C, and D rings and the Cassini Division which separates the A and B rings, extend from 66,900 km ($1.11R_s$) for the inner edge of the D ring to 136,775 km ($2.27R_s$) for the outer edge of the A ring where $1R_s = 60{,}268$ km is the equatorial radius (at the 1 bar atmospheric pressure level) of Saturn. They are thought to be on the order of 10–20 m thick (Charnoz et al., 2009). Prior to the Cassini/Huygens mission, the basic properties of the main ring system, and in particular the normal optical depth (τ_n), were studied by Voyager spacecraft using occultations at radio and ultraviolet wavelengths (Esposito et al., 1983; Holberg et al., 1982; Marouf et al., 1986; Sandel et al., 1982) and in the infrared regime using a ground-based facility (Nicholson et al., 2000). Cassini imaging and occultation data have greatly increased our knowledge and understanding of the rings and their composition and structure. The Radio Science Subsystem, the Visible and Infrared Mapping Spectrometer (VIMS), and the UltraViolet Imaging Spectrograph mapped τ_n (Brown et al., 2004; Colwell et al., 2009; Cuzzi et al., 2009; Nicholson et al., 2008). Comparisons between the different methods have shown a remarkable agreement in τ_n despite the different wavelength regimes and times of the measurements indicating how relatively constant τ_n profile has been over at least 28 years. An

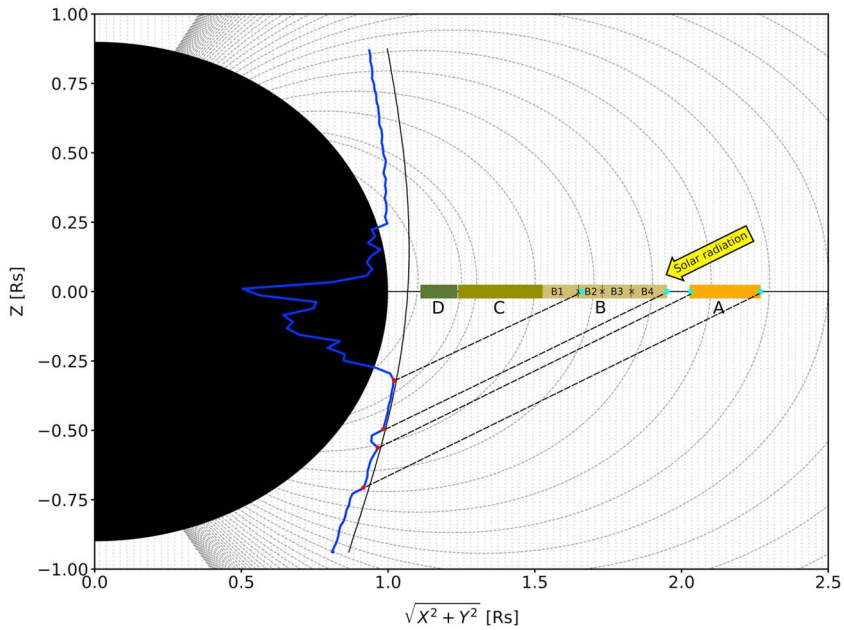

Figure 1. Example of one proximal orbit (Rev 276, 28 May 2017) passing between Saturn (in black) and the rings. The blue curve represents the total direct current for negative bias voltage projected on the orbit. From the observed reduction in the current we could determine the observed boundaries of the shadowed area (delimited by the red dots). The projected boundaries on the ring plane (cyan dots) are compared with the theoretical ring boundaries. Note the constant background current in the northern and southern hemispheres which consists of mainly $I_{ph} + I_{sec}$. It is worth noting that the during the proximal orbits, the altitude varied with latitude.

example of the τ_n profile measured by VIMS is shown in Figure 2b. The observations revealed that the D and C rings are tenuous and optically thin, characterized by a very low τ_n of the order of 10^{-4} and 10^{-1}, respectively (Hedman et al., 2007). The Cassini Division was shown to have a very similar τ_n to the C ring, and the A and B rings to be optically thicker with a larger τ_n, of the order of 1 to 5 for the B ring and around 1 for the A ring (De Pater & Lissauer, 2001). Interestingly, the B ring, which is likely to contain much of the total mass in Saturn's ring system, is characterized by at least four relatively distinct zones (B1 to B4, as shown in Figure 2b) bounded by three major abrupt changes in τ_n (Colwell et al., 2009; Cuzzi et al., 2009; Hedman & Nicholson, 2016; Northrop & Hill, 1983). B1, the innermost zone, extends from the inner edge of the B ring at a radius of 92,000 km to 99,000 km ($1.53R_s$ to $1.64R_s$) and is less opaque with $\tau_n \sim 1$. B2 starts with a sharp increase of τ_n at around 99,000 km ($1.64R_s$) and extends to 104,500 km ($1.73R_s$). It is characterized by a fluctuating region of low and high τ_n varying between ~ 1.5 and > 4. Between around 104,500 and 110,000 km ($1.73R_s$ and $1.83R_s$) lies B3 known as the most opaque zone of Saturn's ring with a median $\tau_n \sim 3.6$ (Colwell et al., 2009; Sandel et al., 1982). B4 is outside 110,000 km ($1.83R_s$) where τ_n decreases to around 2.

Since the A and B rings are optically thick, they are known to cast a shadow on Saturn and its upper atmosphere leading to attenuation of the solar flux. The study of the ring shadowing effects on the ionospheric plasma is essential for a better and complete understanding of the Kronian ionosphere. As the vast majority of Saturn's ionosphere results from the ionization and chemistry of molecular and atomic hydrogen. In addition to photochemistry and plasma diffusion processes, the ring shadowing may also cause variations in the plasma transport and the structure and composition of the ionosphere. Furthermore, since the ion composition highly influences conductivities (Hinson et al., 1998; Moore et al., 2010), the shadows of the rings could also modify the ionospheric conductivity which plays a key role in providing the closure of current systems in the ionosphere. Despite its importance, very few studies have shown the effect of the ring shadows on the ionospheric plasma. Brinkman and McGregor (1979) were the first to calculate the effect of the rings on reducing the solar insolation on Saturn. However, the shadowing effect on the Kronian ionosphere was first explored by Moore et al. (2004) using a time-dependent one-dimensional model of Saturn's ionosphere. They found that the shadows significantly reduce the predicted electron densities.

Our primary objective in this paper is to examine for the first time, using in situ data, the effects of the A and B ring shadows on the Kronian ionosphere and discuss the possible processes that could affect the shadow

signatures in the ionosphere. This is done using the Langmuir probe (LP) data, part of the Radio and Plasma Wave Science (RPWS) investigation from 19 out of 23 proximal orbits of the Cassini Grand Finale.

2. Proximal Orbit Geometry and General Characteristics

On 26 April 2017, the Cassini spacecraft started its last phase of the Grand Finale, by executing a set of 23 proximal orbits passing through the gap between Saturn and its innermost D ring. The orbits had a period of 6.5 days with inclination of 61.7° from the planet's equatorial plane. The closest approach (around 3.9–5.3° south latitude) varied between 4,000 and below 2,000 km in the time period between April and September 2017 (by convention the reference altitude of 0 km is at a pressure of 1 bar).

As Saturn's northern hemisphere experienced summer during the Grand Finale, the planet's northern dayside hemisphere and its rings were fully illuminated by the Sun. However the southern hemisphere was partly obscured because of the shadows cast by the A and B rings, which are opaque to the extreme ultraviolet (EUV) solar radiation (Figure 1). As a consequence, this caused noticeable decrease in the amount of ionization in the southern portion of the ionosphere which were clearly observed by a decrease in the electron densities derived from the RPWS/LP (Hadid et al., 2018; Wahlund et al., 2017) and from the plasma wave frequency characteristics (Persoon et al., 2018) for almost all the proximal orbits at latitudes <−15°.

3. RPWS/LP Method Description

3.1. Measurement Principle

This study is based on the RPWS/LP sweep mode measurements. The LP on board the Cassini spacecraft is a titanium nitride-coated titanium sphere of 5 cm radius. In order to reduce the effect of the photoelectrons ejected from the spacecraft, the probe is installed on a boom so that the sensor is 1.5 m from the nearest spacecraft surface (for a complete description of the RPWS/LP instrument see Gurnett et al., 2004). The LP samples the current of charged particles in two different modes: the voltage sweep and the high-resolution 20-Hz continuous mode.

During the voltage sweep mode the LP samples the total current to the probe each 24 s by sweeping the voltage (U_{bias}) in 512 steps between ±4 V (or ±32 V). The analysis of the sweep data is based on a three-electron Orbit Motion Limited theory (Fahleson et al., 1974; Mott-Smith & Langmuir, 1974), and the current-voltage curves characteristics give estimates of several plasma parameters (the spacecraft potential U_{sc}, the electron number density n_e, the electron temperature T_e, the ion density n_i, the ion ram speed v_i, and the average ion mass m_i; Holmberg et al., 2012; Morooka et al., 2011; Shebanits et al., 2016, 2013; Wahlund et al., 2009). For a sufficiently negative potential, the total current (I_{tot}) can be expressed as the sum of the sampled ion current (I_{i0}), the photoelectron current (I_{ph}) due to the electrons ejected from the probe by EUV radiation, and the secondary electron current (I_{sec}) due to the electrons ejected from the probe (and or the spacecraft) by high energy impacts (Fahleson et al., 1974):

$$I_{\text{tot}} = I_{i0}\left(1 - \frac{U_{\text{float}} + U_{\text{bias}}}{m_i v_i^2/2e}\right) + I_{\text{ph}} + I_{\text{sec}} \tag{1}$$

I_{i0} represents the direct current (DC) level of the ion current and is given by $-\frac{1}{4}en_iA_{\text{LP}}v_i$ where A_{LP} is the surface area of the probe; e is the electron charge; and U_{float}, referred to as the floating potential, represents the spacecraft potential measured at the probe. We note that since the speed, v_i around 31 km/s during the proximal orbits, the thermal current to the probe is negligible compared to the ram current. The continuous sampling mode is performed between the voltage sweeps and measures the electron current at a fixed bias potential of +11.5 V for ±32 V sweep mode (or +4 V for ±4 V sweep mode) with 20 samples per second (Ågren et al., 2009, 2007).

3.2. A and B Ring Boundary Determination

As is shown in equation (1), the total DC ($I_{\text{DC,tot}} = I_{i0} + I_{\text{ph}} + I_{\text{sec}}$) is sensitive to the secondary electrons (I_{sec}) and to the solar EUV photoelectrons (I_{ph}) emitted from the probe (and/or the spacecraft) which give a nearly constant contribution, forming the photoelectron level (≈ −0.7 nA). We note that negligible variation of I_{ph} with the solar EUV flux was observed during the proximal orbits. $I_{\text{DC,tot}}$ is also sensitive to the ambient ions

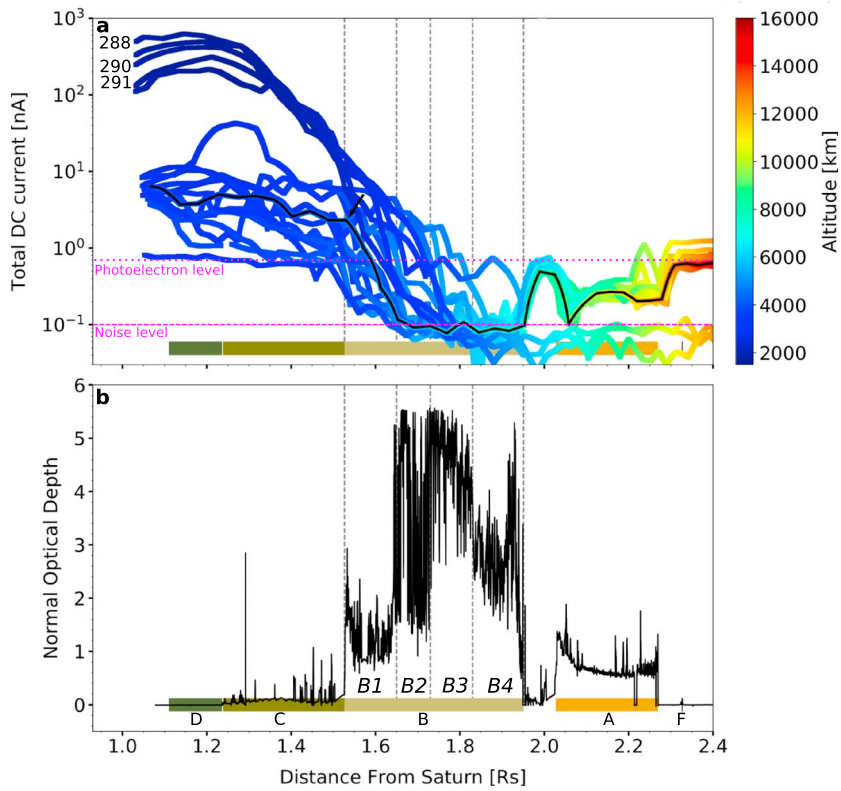

Figure 2. (a) Outbound portions of the interpolated total DC current ($I_{DC,tot}$), projected onto Saturn's ring plane, measured by the LP for 19 proximal orbits. The color code represents the planetographic altitude, and the magenta dashed and dotted lines represent the noise and photoelectron levels of the LP, respectively. (b) normal optical depth (τ_n) of Saturn's main rings derived from stellar occultation (Gam Cru) observed by the Cassini VIMS instrument on 25 August 2008. The main rings are denoted by A, B, C, and D. The gray dashed lines represent the B1 to B4 zones of the B ring. DC = direct current; LP = Langmuir probe; VIMS = Visible and Infrared Mapping Spectrometer.

(I_{i0}) which give an enhancement in the current above the background of photoelectrons. A drop in the total current ($I_{DC,tot}$) below the photoelectron level, down to the noise level of the LP (≈ -0.1 nA), indicates that the probe is not sunlit and so the spacecraft is in a shadowed region. In this way, from the reduction of the ion current and the level of the photoelectron emission during the proximal orbits, we could identify the regions shielded by the opaque A and B rings. As is shown in Figure 1, considering a solar elevation angle of 26.3°, we project that the outbound slant passes onto the ring plane and compare the observed projected boundaries of the shadowed regions (cyan dots) with the ring boundaries.

4. Observations

Using the method described in section 3.2, we interpolate the low time resolution of the LP sweep sampling and project the total DC current ($I_{DC,tot}$) onto the equatorial ring plane for 19 proximal orbits (all but the Final Plunge, Rev 271 [26 April 2017] because of data gap in the LP negative voltage sweeps, Rev 285 [25 July 2017] because the spacecraft was rolling, and Rev 272 [5 February 2017] when the LP was in the wake of the spacecraft during the whole orbit) and compare the shadowed areas with the ring boundaries (Figure 2a). Furthermore, we compare the LP measurements with τ_n values measured by VIMS on 25 August 2008 (Figure 2b). From Figure 2, we find that the total current varies functionally inversely with the ring's opacity and with altitude. Below 4,000 km, beneath the D and C rings, where τ_n is minimal ($\ll 1$), $I_{DC,tot}$ is significantly above the photoelectron level (magenta dotted line) for most of the orbits.

Around 4,000 km, when Cassini is passing below the B ring, which is characterized by a sharp increase of τ_n (> 1), a sudden decrease in $I_{DC,tot}$ can be observed on most of the orbits around the inner edge of the ring ($\sim 1.55R_s$). As an example of this decrease, we show in black orbit 276, which is representative of the other perikrones, except for some of the last orbits (Revs 288, 290, and 291) where $I_{DC,tot}$ decreases more gradually.

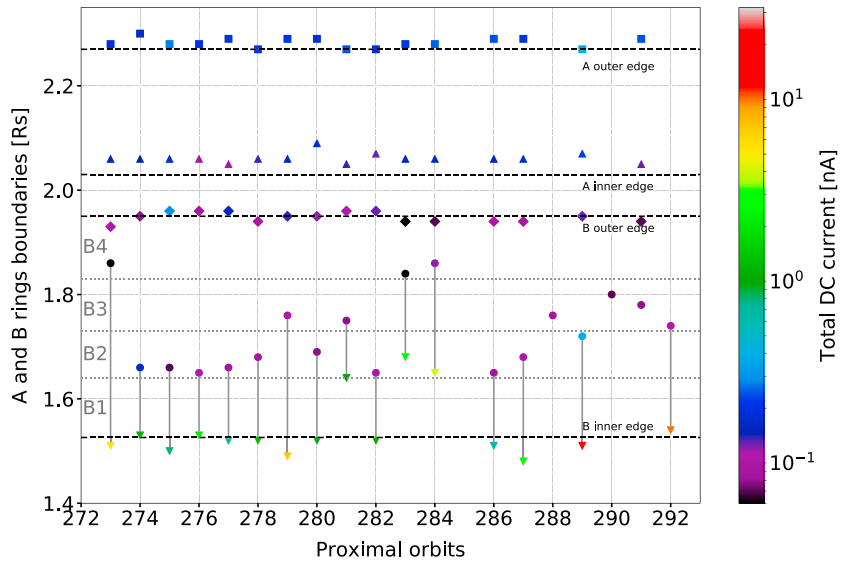

Figure 3. Summary of the observed inner and outer edges of the shadows cast by the A (upward triangles and squares, respectively) and the B rings (circles and diamonds, respectively). The downward triangles correspond to the distance from Saturn when the total DC starts to decrease. The dashed black lines represent the inner and outer boundaries of the A and B rings, and the gray lines represent the B1 to B4 zones in the B ring. The color code corresponds to the total DC. DC = direct current.

Since the B1 region is optically thicker than the D and C rings, $I_{DC,tot}$ would consist of mainly I_{i0} from the ambient ionospheric plasma and partly the currents resulting from the EUV photoelectrons and the secondary electrons ($I_{ph} + I_{sec}$). For distances > 1.65R_s, where Cassini is exiting the B ring at much higher altitudes around 6,000 km and where τ_n increases sharply to larger values, $I_{DC,tot}$ decreases to about the noise level of the LP represented by the magenta dashed line (except for Rev 289 for which the LP was in the wake of the spacecraft at that particular time). Beneath the Cassini Division, a relative increase in $I_{DC,tot}$ can be observed up to around the photoelectron level, except for Revs 288, 290, and 292 for which the Langmuir probe was shadowed by the spacecraft. When passing below the A ring, $I_{DC,tot}$ decreases again below the photoelectron level but still higher than the noise level ($\sim$ 0.3 nA). It is worth noting that clear dips in $I_{DC,tot}$ are observed on all the perikrones when passing below the A ring, consistent with the increase of τ_n at the inner part of the ring (Figure 2b). Finally, at higher altitudes outside the A ring ($\gtrsim$ 12,000 km), $I_{DC,tot}$ increases back to the photoelectron level, consistent with the sharp decrease of τ_n.

In Figure 3 we summarize the distances of the observed starting and ending points of the shadows compared with the A and B ring boundaries (black dashed lines). The color code represents the total DC current. Based on the current values, we consider the LP in complete shadow when the collected current is below the photoelectron level (< 0.7 nA) and around the noise level (0.1 nA, purple in the color bar). As one can see, the observed edges of the shadow cast by the A ring (squares and upward triangles) are in agreement with its boundaries. This is observed consistently on all the orbits, although a slight outward shift ($\sim$ 3,600 km) occurs at the inner edge (upward triangles). This offset could be due to a fine structure of the rings or a variable shape of the Cassini Division, due to various moon resonances (Hedman et al., 2010). In order to confirm this effect, a much more detailed study is required. Regarding the B ring, the observed outer edges of the shadow (diamonds) match the outer edge of the ring consistently from one orbit to another. However, this is not the case for the inner edges of the shadow (circles); which are neither uniform nor matching the B ring inner boundary. For each orbit, we represent by a downward triangle the distance at which $I_{DC,tot}$ suddenly starts to decrease, represented by a *knee* in $I_{DC,tot}$, defined by the point after which a clear increase in the slope of the current occurs (as pointed by the arrow in Figure 2a for one of the perikrones). Moreover, we represent by a circle the distance at which the LP is shadowed by the B ring ($I_{DC,tot} \sim 0.1$ nA). Regarding Revs 288, 290, and 291 (labeled in Figure 2a) we do not define any starting point of the current decrease, since the change in the current slope could not be clearly observed. For most the orbits, $I_{DC,tot}$ starts to decrease around the inner edge of the B ring. However, it reaches the noise level at least around 1.65*Rs* (the inner edge of B2 zone) for the majority of

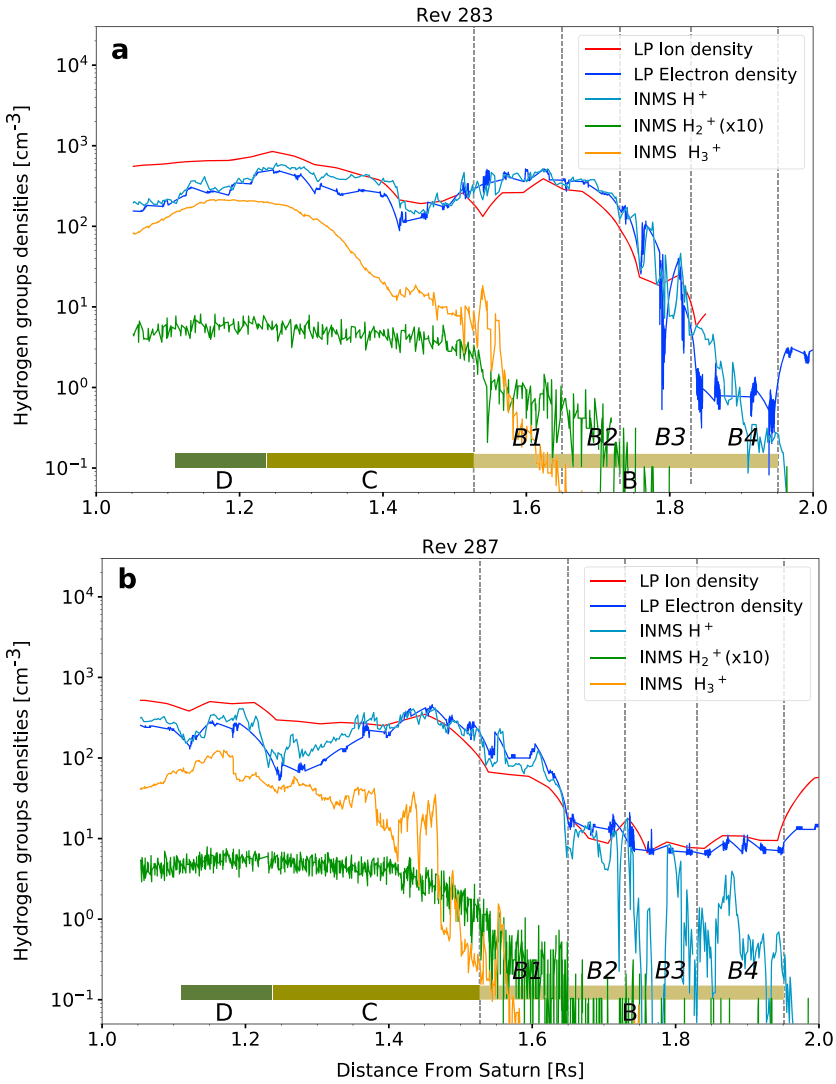

Figure 4. LP electron (dark blue) and ion densities (red) and INMS H^+ (light blue), 10xH_2^+ (green), and H_3^+ (orange) densities projected on the ring plane for two examples of the proximal orbits, Rev 283 (a) and Rev 287 (b). The mismatch between INMS H^+ density and the LP ion and electron densities in Rev 287 (b) for distances > 1.7 Rs is due to the photoelectrons emitted by the LP and/or the spacecraft. LP = Langmuir probe; INMS = Ion and Neutral Mass Spectrometer.

the orbits, where the optical depth increases sharply (Figure 2). We note that for few cases (Revs 273, 283, and 284), $I_{DC,tot}$ reaches the noise level in the outer part of the ring around 1.83 R_s.

In order to understand the variations in the starting point of the B ring shadow, we present in Figure 4 the electron densities measured by the LP (dark blue) and the molecular hydrogen group densities, H^+, measured by the LP and Ion and Neutral Mass Spectrometer (INMS; red and light blue, respectively), 10xH_2^+, and H_3^+ from INMS (green and orange, respectively). We compare the measurements for two perikrones: Rev 283 and Rev 287. For both cases the electron and H^+ densities from the LP and INMS are consistent with each other and dominate over H_2^+ and H_3^+ confirming the importance of H^+ in this region. Moreover, one can see that the electron and H^+ densities decrease more slowly than H_2^+ and H_3^+ densities in both examples, implying the longer chemical lifetime of H^+ compared to the one of H_2^+ and H_3^+. Despite those similarities, clear differences exist between the two orbits. First, as already shown in Figure 3, for Rev 283 (Figure 4a), the B ring shadowing signature, shown by the sharp decrease of H^+ and the electron densities, occurs at the outer edge of B3 zone unlike Rev 287 where the shadow starts earlier, at the outer edge of B1 zone. Additionally, one can note that for Rev 283, where the shadowing effect is delayed, H_3^+ and in particular H_2^+ densities decrease to ~ 0.1 cm^{-3}

(0.01 cm^{-3} as the real value) around the outer edge of B2 zone, whereas for Rev 287 for which the shadow starts earlier, H_3^+ and H_2^+ densities reach the same value within the B1 zone. It is worth noting that the real noise level value of INMS is around $\sim$ 0.01 cm^{-3}. This suggests that the H^+ response to the shadowing effect is directly related to the H_2^+ response which is expected to be much faster.

5. Discussion

The RPWS/LP in situ measurements during Cassini's Grand Finale show a clear effect of the main rings on the structure of the Kronian topside ionosphere, consistently on the 19 analyzed orbits. An inverse correlation between $I_{DC,tot}$ and the ring opacity is observed (Figure 2b). As expected, this is a direct result of the solar flux reduction from the rings which hence modifies the photoionization rate of the molecular and atomic hydrogen, the dominant constituents in Saturn's upper atmosphere. No shadowing effects from the tenuous D and C rings are observed, consistent with their relative transparency to the EUV solar radiation (Colwell et al., 2009). An inverse correlation between the A, B, and C rings, the Cassini Division, and the electron density has been shown previously by Farrell et al. (2017), during the Cassini Saturn orbit insertion period in 2004. This inverse trend has been also reported by Coates et al. (2005) for the A ring and the Cassini Division and suggested by models (Bouhram et al., 2006; Tseng et al., 2013).

Moreover, clear differences between the observed A and B rings shadows are reported. The reduction in $I_{tot,DC}$ caused by the A ring shadow is observed uniformly on all the perikrones and is in agreement with the inner and outer edges of the A ring (Figure 3). Regarding the B ring shadow, unlike its ending point, its starting point does not correspond to the inner edge of the ring and varies from one orbit to another, although its lowest optical depth value is similar to the optical depth of the A ring (Figure 2a). This is very much tied to the altitude-latitude variation of each of the proximal orbits (Hadid et al., 2018; Persoon et al., 2018; Wahlund et al., 2017). In fact, for altitudes $\lesssim$ 4,000 km, the spacecraft enters the region which is shadowed by the B ring where the plasma is still relatively dense, around 100 cm^{-3} as shown in Hadid et al. (2018) and Persoon et al. (2018). As a consequence the collected ion current will dominate over the photoelectron and secondary electron current. However, at higher altitudes >8,000 km, when Cassini approaches beneath the A ring shadow in the plasmasphere, the plasma density is much smaller, $\lesssim$ 10 cm^{-3} (Hadid et al., 2018; Persoon et al., 2018), because of the low proton production rate (Moore et al., 2004). As a result, the total collected current, consisting of mainly the photoelectron and the secondary electron current, would react instantaneously to the ring shadow when the sunlight is *turned off*.

The observed variations in the starting point of the B ring shadow around 4,000 km, to distances outside 1.65R_s (notably for Rev 273, 283, and 284), are most probably related to the ionospheric plasma and in particular to the changes of the proton production rate resulting in different responses of the molecular hydrogen to the shadows in the ionosphere. As shown in Figure 4 using INMS and the LP measurements, the H^+ densities respond slower to the shadowing effects compared to H_3^+ and H_2^+ for which the response is much faster as expected. Since at those latitudes/altitudes the photochemical equilibrium does not hold anymore (Cravens et al., 2018; chemical timescales become larger than transport timescales), this suggests that the plasma produced outside the shadow is transported into the shadowed region. Moreover, the responses of the H_2^+ to the shadow are shown to be different. Unlike Rev 287, for Rev 283 the response is delayed, and as a consequence the response of H^+ is delayed. This has been confirmed recently by Waite et al. (2018) who showed similar results by comparing quantitatively the densities of the molecular hydrogen groups for Rev 288 using INMS data. Moreover, Moore et al. (2004) had also reported, using a model of the Kronian ionosphere, that H^+ responds more slowly to the shadowing effects as it has a longer lifetime compared to H_3^+ resulting in a delayed shadowing effect. Other than the ionospheric plasma, an influx of D and C ring material along the field lines (Ip, 1984; Tseng et al., 2013, 2010) could also drive the chemistry of the Kronian ionosphere in the shielded region and so modify the shadowing signatures in the ionosphere. Unfortunately, since at the spacecraft speed of 31 km/s INMS measurements were limited to masses of 8 amu, it could not measure and verify the presence of any ring ions, such as O^+, H_2O^+, or O_2^+ (Waite et al., 2018). Finally, the total DC current collected by the LP nicely reproduces some of the optical depth properties of the rings. In particular, the higher optical depths of the inner part of the A ring compared to the rest of the ring (Figure 2a) translates in the LP measurements by a decrease of the total current at the inner part of the ring (Figure 2b). Regarding the B ring, since none of the shadows start below 1.65 R_s, this suggests that the inner part of this ring opaque than the outer part, consistent with the B1 zone of the ring. Moreover, for altitudes >7,000 km, the total current

in the outer part of the B ring (B4) reaches the noise level of the LP unlike for the A ring (Figure 2b). This is in agreement with the lower optical depth of the A ring compared to B4 and highlights the measurement constraints of the LP at those specific high altitudes.

6. Conclusions

In summary, using the RPWS/LP in situ measurements, we could trace some of the optical properties of the rings and show the role of the transported ionospheric plasma in modifying the ionospheric shadow signatures from the B ring. At high altitude (>7,000 km) where the plasma is tenuous ($\leq$ 10 cm^{-3}), clear and consistent shadowing is observed from the A ring. At lower altitudes ($\sim$ 4,000 km) where the plasma is dense ($\geq$ 100 cm^{-3}), variable responses of the ionosphere to the B ring shadowing are observed. We show that this variation is due to the changes in the proton production rate and to the longer chemical lifetime of H^+, compared to H_2^+ and H_3^+, suggesting that it is transported from the sunlit to the shadowed regions in the ionosphere.

Acknowledgments
The RPWS/LP instrument on board Cassini is supported by the Swedish National Space Board (SNSB). L. Z. H. acknowledges funding by the Swedish Research Council (Vetenskapsrådet, VR) under the contract 2016-05364. M. W. M. acknowledges funding by the SNSB under contract 174/15. N. J. T. E. acknowledges funding by the SNSB under contract 135/13 and VR under contract 621-2013-4191. L. M. acknowledges support from the National Aeronautics and Space Administration under grant NNX16AI34G issued through the Cassini Data Analysis Program. The research at the University of Iowa was supported by NASA through contract 1415150 with the Jet Propulsion Laboratory. Cassini RPWS data will be available on NASA Planetary Data System https://pds.jpl.nasa.gov.

References

Ågren, K., Wahlund, J.-E., Garnier, P., Modolo, R., Cui, J., Galand, M., & Muller-Wodarg, I. (2009). On the ionospheric structure of Titan. *Planetary and Space Science*, *57*, 1821–1827. https://doi.org/10.1016/j.pss.2009.04.012

Ågren, K., Wahlund, J.-E., Modolo, R., Lummerzheim, D., Galand, M., Müller-Wodarg, I., et al. (2007). On magnetospheric electron impact ionisation and dynamics in Titan's ram-side and polar ionosphere—A Cassini case study. *Annales Geophysicae*, *25*, 2359–2369. https://doi.org/10.5194/angeo-25-2359-2007

Bouhram, M., Johnson, R. E., Berthelier, J.-J., Illiano, J.-M., Tokar, R. L., Young, D. T., & Crary, F. J. (2006). A test-particle model of the atmosphere/ionosphere system of Saturn's main rings. *Geophysical Research Letters*, *33*, L05106. https://doi.org/10.1029/2005GL025011

Brinkman, A. W., & McGregor, J. (1979). The effect of the ring system on the solar radiation reaching the top of Saturn's atmosphere: Direct radiation. *Icarus*, *38*, 479–482. https://doi.org/10.1016/0019-1035(79)90202-1

Brown, R. H., Baines, K. H., Bellucci, G., Bibring, J.-P., Buratti, B. J., Capaccioni, F., et al. (2004). The Cassini visible and infrared mapping spectrometer (VIMS) investigation, *The Cassini-Huygens mission: Orbiter Remote Sensing Investigations* (pp. 111–168). Netherlands: Springer. https://doi.org/10.1007/1-4020-3874-7_3

Charnoz, S., Dones, L., Esposito, L. W., Estrada, P. R., & Hedman, M. M. (2009). Origin and evolution of Saturn's ring system. *Saturn from Cassini-Huygens* (pp. 537–575). Netherlands: Springer. https://doi.org/10.1007/978-1-4020-9217-6_17

Coates, A. J., McAndrews, H. J., Rymer, A. M., Young, D. T., Crary, F. J., Maurice, S., et al. (2005). Plasma electrons above Saturn's main rings: CAPS observations. *Geophysical Research Letters*, *32*, L14S09. https://doi.org/10.1029/2005GL022694

Colwell, J. E., Nicholson, P. D., Tiscareno, M. S., Murray, C. D., French, R. G., & Marouf, E. A. (2009). The structure of Saturn's rings. *Saturn from Cassini-Huygens* (pp. 375–412). Netherlands: Springer. https://doi.org/10.1007/978-1-4020-9217-6_13

Cravens, T. E., Moore, L., Waite, J. H. Jr., Perryman, R., Perry, M., Wahlund, J.-E., et al. (2018). The ion composition of Saturn's equatorial ionosphere as observed by Cassini. *Geophysical Research Letters*, *45*. https://doi.org/10.1029/2018GL077868

Cuzzi, J., Clark, R., Filacchione, G., French, R., Johnson, R., Marouf, E., & Spilker, L. (2009). Ring particle composition and size distribution. *Saturn from Cassini-Huygens* (pp. 459–509). Netherlands: Springer. https://doi.org/10.1007/978-1-4020-9217-6_15

De Pater, I., & Lissauer, J. J. (2001). *Planetary Sciences*. Cambridge University Press. https://doi.org/10.1017/CBO9781316165270

Esposito, L. W., O'Callaghan, M., Simmons, K. E., Hord, C. W., West, R. A., Lane, A. L., et al. (1983). Voyager photopolarimeter stellar occultation of Saturn's rings. *Icarus*, *88*, 8643–8649. https://doi.org/10.1029/JA088iA11p08643

Fahleson, U., Fälthammar, C.-G., & Pedersen, A. (1974). Ionospheric temperature and density measurements by means of spherical double probes. *Planetary and Space Science*, *22*, 0032–0633. https://doi.org/10.1016/0032-0633(74)90122-6

Farrell, W. M., Kurth, W. S., Gurnett, D. A., Persoon, A. M., & MacDowall, R. J. (2017). Saturn's rings and associated ring plasma cavity: Evidence for slow ring erosion. *Icarus*, *292*, 48–53. https://doi.org/10.1016/j.icarus.2017.03.022

Gurnett, D. A., Kurth, W. S., Kirchner, D. L., Hospodarsky, G. B., Averkamp, T. F., Zarka, P., et al. (2004). The Cassini radio and plasma wave investigation. *Space Science Reviews*, *114*, 395–463. https://doi.org/10.1007/s11214-004-1434-0

Hadid, L. Z., Morooka, M. W., Wahlund, J.-E., Persoon, A. M., Andrews, D. J., Shebanits, O., et al. (2018). Saturn's ionosphere: Electron density altitude profiles and D ring interaction from the Cassini Grand Finale. *Geophysical Research Letters*, *45*. https://doi.org/10.1029/2018GL078004

Hedman, M. M., Burns, J. A., Showalter, M. R., Porco, C. C., Nicholson, P. D., Bosh, A. S., et al. (2007). Saturn's dynamic D ring. *Icarus*, *188*, 89–107. https://doi.org/10.1016/j.icarus.2006.11.017

Hedman, M. M., & Nicholson, P. D. (2016). The B-ring's surface mass density from hidden density waves: Less than meets the eye? *Icarus*, *279*, 109–124. https://doi.org/10.1016/j.icarus.2016.01.007

Hedman, M. M., Nicholson, P. D., Baines, K. H., Buratti, B. J., Sotin, C., Clark, R. N., et al. (2010). The architecture of the Cassini division. *The Astronomical Journal*, *139*, 228–251.

Hinson, D. P., Twicken, J. D., & Karayel, E. T. (1998). Jupiter's ionosphere: New results from Voyager 2 radio occultation measurements. *Journal of Geophysical Research*, *103*(A5), 9505–9520. https://doi.org/10.1029/97JA03689

Holberg, J. B., Forrester, W. T., & Lissauer, J. J. (1982). Identification of resonance features within the rings of Saturn. *Nature*, *297*, 115–120. https://doi.org/10.1038/297115a0

Holmberg, M. K. G., Wahlund, J.-E., Morooka, M. W., & Persoon, A. M. (2012). Ion densities and velocities in the inner plasma torus of Saturn. *Planetary and Space Science*, *73*(1), 151–160. https://doi.org/10.1016/j.pss.2012.09.016

Ip, W.-H. (1984). Electrostatic charging of the rings of Saturn: A parameter study. *Journal of Geophysical Research*, *89*(A6), 3829–3836. https://doi.org/10.1029/JA089iA06p03829

Marouf, E. A., Leonard, T. G., & Rosen, P. A. (1986). Profiling Saturn's rings by radio occultation. *Icarus*, *68*, 120–166. https://doi.org/10.1016/0019-1035(86)90078-3

Moore, L. E., Mendillo, M., M uller-Wodarg, I. C. F., & Murr, D. L. (2004). Modeling of global variations and ring shadowing in Saturn's ionosphere. *Icarus*, *172*, 503–520. https://doi.org/10.1016/j.icarus.2004.07.007

Moore, L. E., Mueller-Wodarg, I., Galand, M., Kliore, A., & Mendillo, M. (2010). Latitudinal variations in Saturn's ionosphere: Cassini measurements and model comparisons. *Journal of Geophysical Research*, *115*, A11317. https://doi.org/10.1029/2010JA015692

Morooka, M. W., Wahlund, J.-E., Eriksson, A. I., Farrell, W. M., Gurnett, D. A., Kurth, W. S., et al. (2011). Dusty plasma in the vicinity of Enceladus. *Journal of Geophysical Research*, *116*, A12221. https://doi.org/10.1029/2011JA017038

Mott-Smith, H. M., & Langmuir, I. (1974). The theory of collectors in gaseous discharges. *Physical Review*, *28*, 727–763. https://doi.org/10.1103/PhysRev.28.727

Nicholson, P. D., French, R. G., Tollestrup, E., Cuzzi, J. N., Harrington, J., Matthews, K., et al. (2000). Saturn's rings I: Optical depth profiles from the 28 Sgr occultation. *Icarus*, *145*, 474–501. https://doi.org/10.1006/icar.2000.6356

Nicholson, P. D., Hedman, M. M., Clark, R. N., Showalter, M. R., Cruikshank, D. P., Cuzzi, J. N., et al. (2008). A close look at Saturn's rings with Cassini VIMS. *Icarus*, *193*, 182–212. https://doi.org/10.1016/j.icarus.2007.08.036

Northrop, T. G., & Hill, J. R. (1983). The inner edge of Saturn's B ring. *Journal of Geophysical Research*, *A8*(88), 6102–6108. https://doi.org/10.1029/JA088iA08p06102

Persoon, A. M., Kurth, W. S., Gurnett, D. A., Groene, J. B., Sulaiman, A., Wahlund, J.-E., et al. (2018). Electron density distributions in Saturn's ionosphere. *Geophysical Research Letters*, *45*. https://doi.org/10.1029/2018GL078020

Sandel, B. R., Shemansky, D. E., Broadfoot, A. L., Holberg, J. B., Smith, G. R., Mcconnell, J. C., et al. (1982). Extreme ultraviolet observations from the Voyager 2 encounter with Saturn. *Science*, *215*, 548–553. https://doi.org/10.1126/science.215.4532.548

Shebanits, O., Wahlund, J.-E., Edberg, N. J. T., Crary, F. J., Wellbrock, A., Andrews, D. J., et al. (2016). Ion and aerosol precursor densities in Titan's ionosphere: A multi-instrument case study. *Journal of Geophysical Research: Space Physics*, *121*, 10,075–10,090. https://doi.org/10.1002/2016JA022980

Shebanits, O., Wahlund, J.-E., Mandt, K., Ågren, K., Edberg, N. J. T., & Waite, J. H. (2013). Negative ion densities in the ionosphere of Titan-Cassini RPWS/LP results. *Planetary and Space Science*, *84*, 153–162. https://doi.org/10.1016/j.pss.2013.05.021

Tseng, W.-L., Johnson, R. E., & Elrod, M. K. (2013). Modeling the seasonal variability of the plasma environment in Saturn's magnetosphere between main rings and Mimas. *Planetary and Space Science*, *77*, 126–135. https://doi.org/10.1016/j.pss.2012.05.001

Tseng, W.-L., Johnson, R. E., Thomsen, M. F., Cassidy, T. A., & Elrod, M. K. (2010). Neutral H_2 and H_2^+ ions in the Saturnian magnetosphere. *Journal of Geophysical Research*, *116*, A03209. https://doi.org/10.1029/2010JA016145

Wahlund, J.-E., André, M., Eriksson, A. I. E., Lundberg, M., Morooka, M. W., Shafiq, M., et al. (2009). Detection of dusty plasma near the E-ring of Saturn. *Planetary and Space Science*, *14*(57), 1795–1806. https://doi.org/10.1016/j.pss.2009.03.011

Wahlund, J-E., Morooka, W. M, Hadid, L. Z., Persoon, A. M., Farrell, W. M., Gurnett, D. A., et al. (2017). In situ measurements of Saturn's ionosphere show that it is dynamic and interacts with the rings. *Science*, *359*, 66–68. https://doi.org/10.1126/science.aao4134

Waite, J. H. Jr., Perryman, R., Perry, M., Miller, K., Bell, J., Cravens, T. E., et al. (2018). INMS observations of chemical interactions between Saturn's atmosphere and rings. *Science*, https://doi.org/10.1126/science.aat2382